Supporting Information

Szyszka et al. 10.1073/pnas.1412051111

SI Materials and Methods

We estimated the proportion of odorant molecules that could reach the ORN dendrite within 1 ms via diffusion as follows: We assumed a molecular mass of 15 kDa for the odorant/OBP complex (1) and estimated a radius r of 1.63 nm according to established relationships between volume and molecular mass for folded proteins (2). By reference to reported values for other aqueous biological solutions, we assumed a dynamic viscosity η of sensillum lymph of 0.002 Pa·s. The distance d between the ORN dendrite and sensillum pore was taken to be 0.3 μm (3). Using the Stokes–Einstein equation, the diffusion constant $D = k \times T/(6 \times \pi \times \eta \times r)$, where k is Boltzmann's constant and T is the temperature during experiments (25° C = 298 K). Plugging in the values above gives $D \sim 5 \times 10^{-11}$ $m^2 \cdot s^{-1}$. Concentration at distance x in a profile along the dimension of interest evolves according to $\langle x^2 \rangle^{1/2} = (2 \times D \times t)^{1/2}$, where $\langle x^2 \rangle^{1/2}$ is the SD of the displacement. At $t = 1$ ms, this distance equals ∼0.316 μm. Taking this value as the SD, and a target distance of 0.3 microns, the inverse normal cumulative distribution function yields a quantile of 0.171, implying that 17.1% of the molecules will have reached the target after 1 ms. Simulation using difference equations and applying the actual boundary conditions ($0 < x < 0.3$ μm) gives an even larger proportion.

1. Vogt RG, Riddiford LM (1981) Pheromone binding and inactivation by moth antennae. *Nature* 293(5828):161–163.
2. Erickson HP (2009) Size and shape of protein molecules at the nanometer level determined by sedimentation, gel filtration, and electron microscopy. *Biol Proced Online* 11(1):32–51.
3. Shanbhag SR, Muller B, Steinbrecht RA (1999) Atlas of olfactory organs of Drosophila melanogaster - 1. Types, external organization, innervation and distribution of olfactory sensilla. *Int J Insect Morphol* 28(4):377–397.

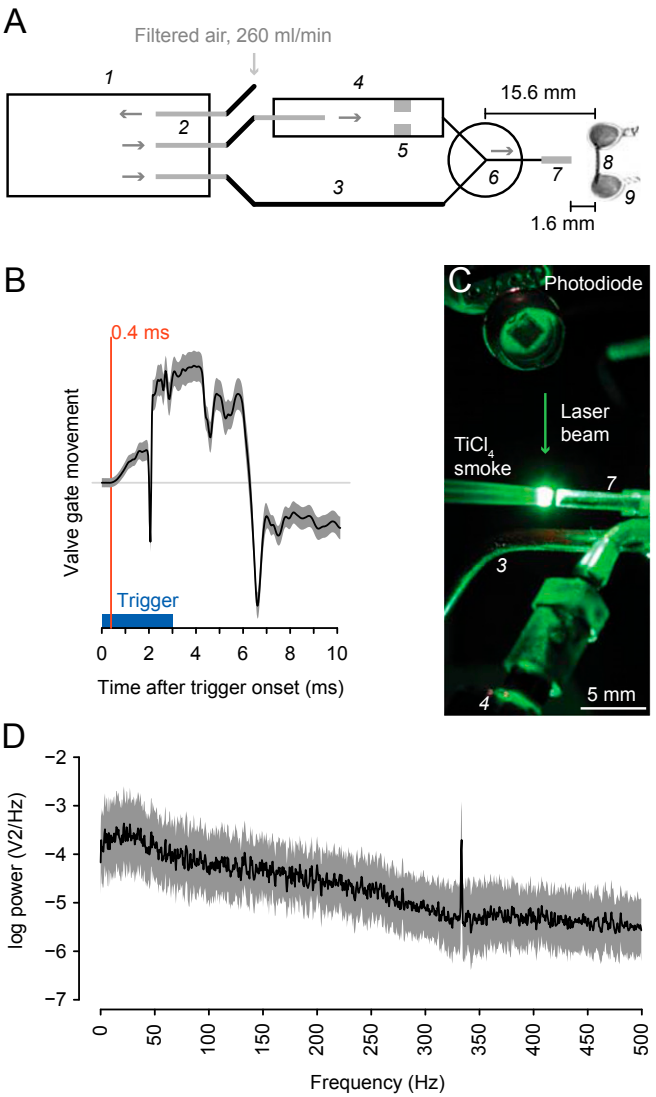

Fig. S1. The odor delivery device. (*A*) Scheme of the odor delivery device. 1, glass vial with Teflon septum, 20 mL; 2, injection needle, 1.2 × 40 mm; 3, tygon tube, 1 mm inner diameter; 4, plastic syringe, 2.5 mL; 5, cellulose strip with odorant; 6, three-way solenoid valve; 7, steel tube, 1.2 mm inner diameter; 8, antenna; 9, electrode. (*B*) Movement of the gate that opens the valve. The valve starts moving 0.4 ms after the electrical trigger signal measured by directing a laser beam onto the gate and measuring the reflected light with a photodiode. (*C*) Odor arrival at the antenna was visualized with $TiCl_4$ smoke. A laser was positioned perpendicular to the airflow at the location of the antenna, and the resulting light reflectance of the $TiCl_4$ smoke was recorded with a photodiode. Numbers refer to *A*. (*D*) Periodogram of $TiCl_4$ smoke signals during the final 9 s of the broadband stimulus (mean ± SD, $n = 12$).

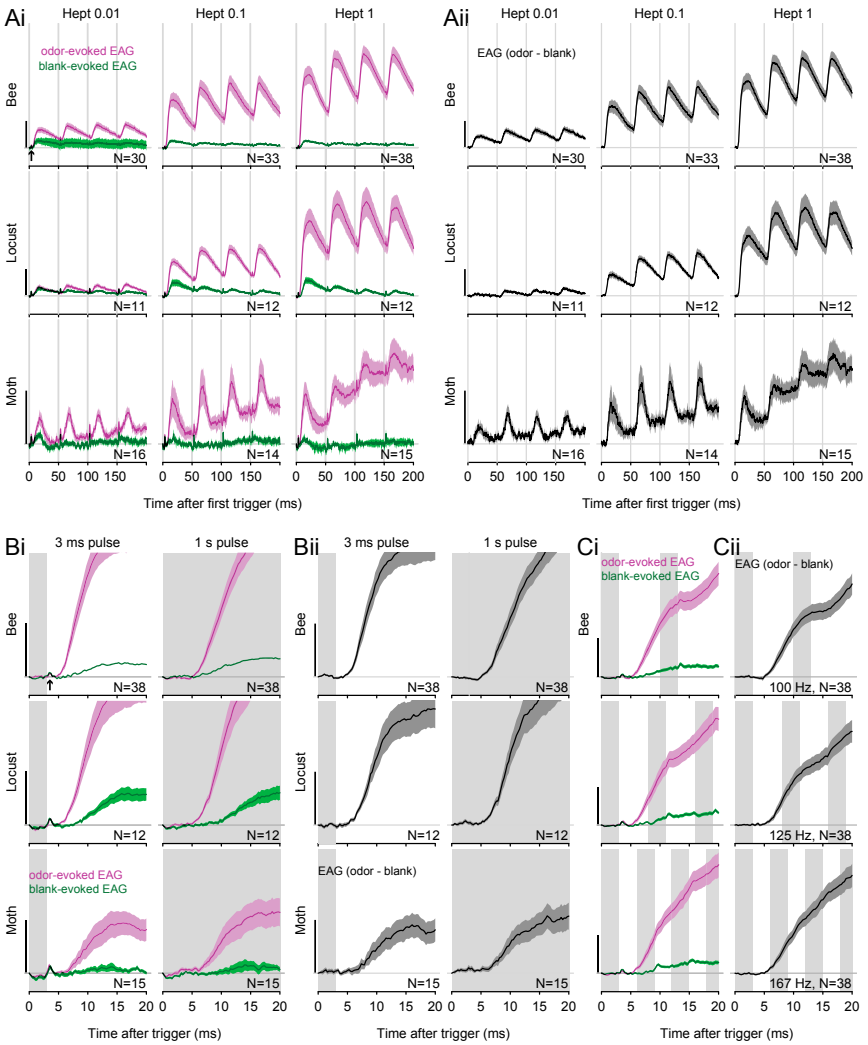

Fig. S2. Calculation of odor-evoked EAG responses. To exclude nonolfactory EAG signals, odor and blank control stimuli were alternated, and blank-evoked EAG signals (green) were subtracted from odor-evoked EAG signals (magenta). (*A*) EAG responses to 3-ms pulses of 2-heptanone delivered at 20-Hz pulses (gray vertical bars) and at different concentrations. The odor delivery device produced a short stimulus artifact (arrowhead) that coincided with the offset of the valve trigger. The stimulus artifact was visible in the odor-evoked and blank evoked EAG signal (*Ai*), but not in the subtracted EAG responses (*Aii*). (*B*) EAG responses to 3-ms and 1-s-long pulses of undiluted 2-heptanone. The stimulus artifact evoked by the stimulus offset, because it was visible 3 ms after the onset of 3-ms pulses but not after the onset of 1-s pulses (*Bi*). The stimulus artifact was not visible in the subtracted EAG responses (*Bii*). (*C*) Honey bee EAG responses to 3-ms pulses of undiluted 2-heptanone delivered at 100, 125, and 167 Hz (gray vertical bars) before (*Ci*) and after (*Cii*) subtraction of the blank-evoked EAG signal. Odor-evoked EAG response could follow 125-Hz but not 167-Hz pulses (compare with power spectra in Fig. 3*A*). (Scale bars: 0.2 mV.)

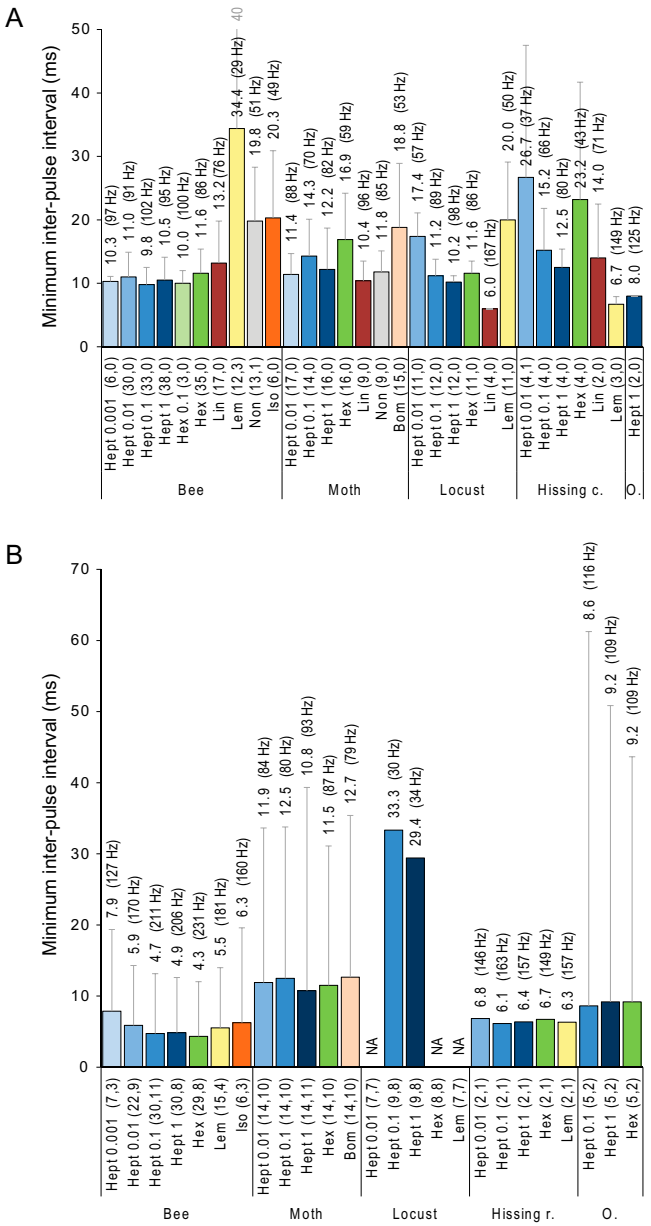

Fig. S3. Across-antenna variability of maximal temporal resolution of EAG responses. (*A*) Temporal resolution during a 1-s-long fixed frequency pulse train. Mean and SD of minimum resolvable interpulse intervals across antennae. Minimum resolvable interpulse interval (1/maximum pulse frequency) was ascertained if the value of the odor-evoked periodogram at the stimulus frequency was two times higher than the surrounding baseline ± 20 Hz. Odor-evoked periodograms were calculated for single recordings by taking the periodogram of the EAG response to the odor stimulus and subtracting the corresponding periodogram of the "blank" air EAG response. Numbers in the graph show the mean resolvable interpulse interval (1/frequency), and the corresponding pulse tracking frequencies are given in parentheses. The gray number above the graph shows the actual value of the truncated SD. At the *x*-axis label, the first value in the parentheses indicates the total number of antennae, the second value indicates the number of antennae in which no response onset or minimum interpulse interval could be detected. (*B*) Temporal resolution during a 10-s-long broadband frequency pulse train. Mean and SD of minimum resolvable interpulse intervals across antennae. Minimum resolvable interpulse intervals were determined as in Fig. 4 *B* and *C*, except that the coherence between EAG response and $TiCl_4$ smoke signal was calculated for each single antenna. Numbers in the graph show the mean resolvable interpulse interval, and the corresponding pulse tracking frequencies are given in parentheses. The first value in the parentheses indicates the total number of antennae; the second value indicates the number of antennae in which no minimum interpulse interval could be detected.

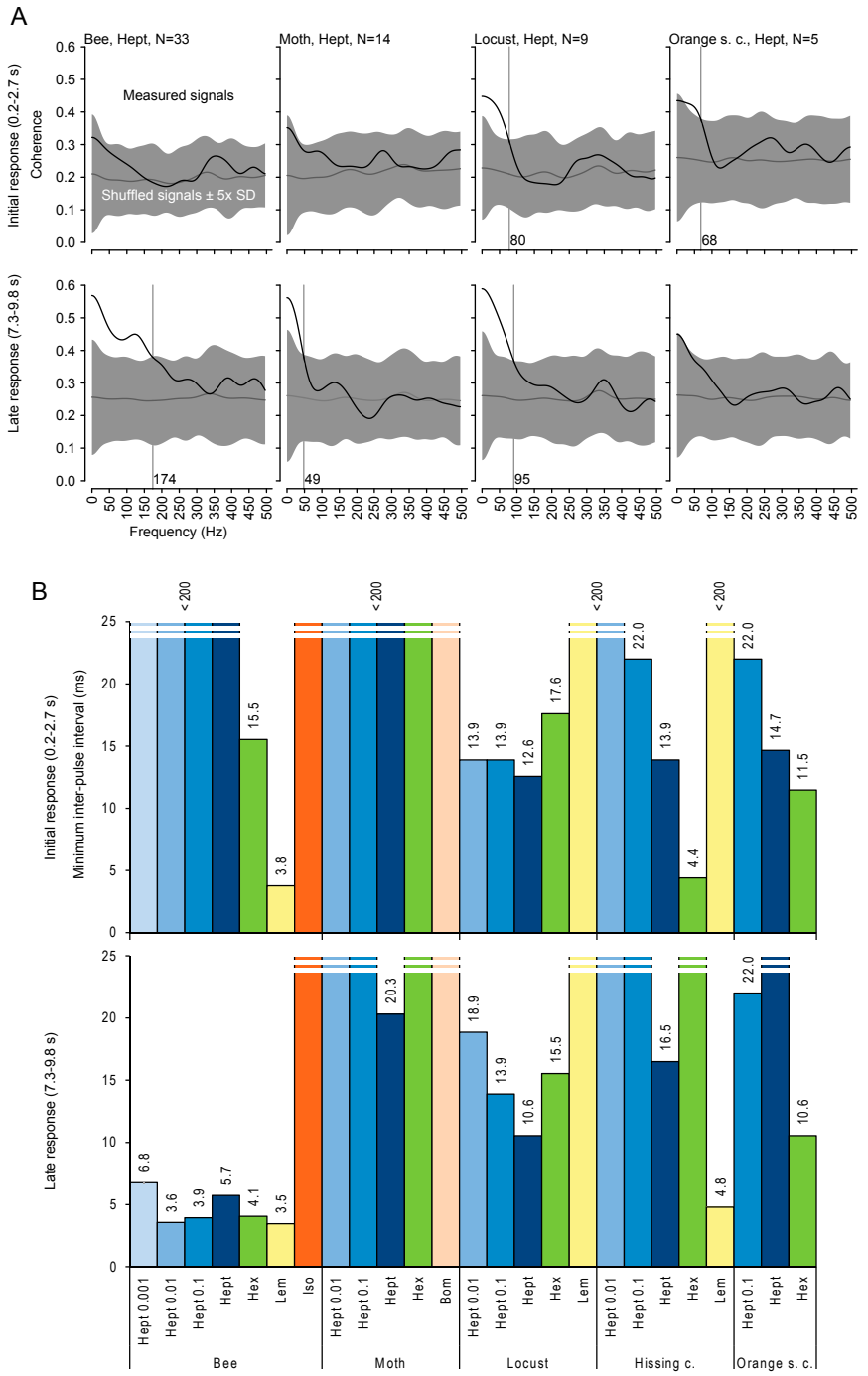

Fig. S4. Temporal resolution of EAG responses during initial and late odor responses. (*A*) Coherence between EAG responses and smoke signals measured during the initial (0.2–2.7 s) and late (7.3–9.8 s) period of a 10-s-long broadband frequency stimulus train with random pulse durations. The values at the vertical lines show the maximum EAG frequency responses with significant coherence. (*B*) Temporal resolution of EAG responses quantified as the minimum interpulse interval (1/maximum pulse frequency) at which the coherence is still significant.

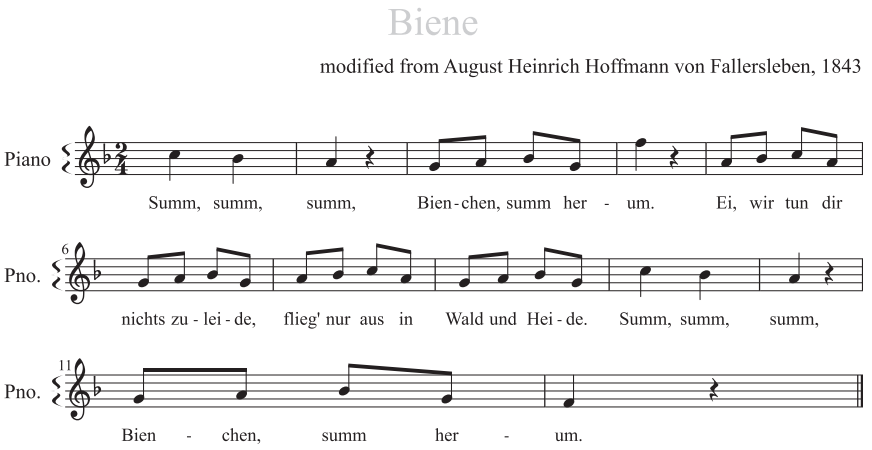

Fig. S5. Children's song "Biene" by August Heinrich Hoffmann von Fallersleben, 1843. The note "F4" was replaced by "F5" to get a wider frequency range. Sheet music was generated in Musescore (musescore.org).

Audio File S1. Children`s song "Biene." The audio file was generated in Musecore.

Audio File S1

Audio File S2. The song "Biene" transposed to notes in the 100- to 200-Hz range and played with the valve of the odor delivery device. Note that the song stopped prematurely in the second-to-last measure because of configuration of the stimulation software.

Audio File S2

Audio File S3. Odor-evoked EAG responses during the presentation of the song "Biene" with the odor delivery device (mean of 2 bee and 2 moth antennae, 40–400 Hz band-pass filtered).

Audio File S3